Wang et al. Nanoscale Research Letters (2017) 12:145
DOI 10.1186/s11671-017-1924-0

Nanoscale Research Letters

NANO EXPRESS

Open Access

Selective-Area Growth of Transferable InN Nanocolumns by Using Anodic Aluminum Oxide Nanotemplates

Xiao Wang*, Guozhen Zhang, Yang Xu, Hao Wu and Chang Liu

Abstract

InN nanocolumn arrays were grown on c-plane sapphire with and without anodic aluminum oxide (AAO) nanotemplates. The crystalline quality of InN nanocolumns was significantly improved by selective-area growth (SAG) using AAO templates, as verified by X-ray diffraction measurements. Then, InN nanocolumns were transferred onto p-type silicon substrates after etching off the AAO templates. Current–voltage characteristic of the transferred n-InN/p-Si heterojunctions shows on/off ratio as high as 4.65×10^3 at 2 V. This work offers a potential way to grow transferable devices with improving performances.

Keywords: InN nanocolumns, Anodic aluminum oxide, Selective-area growth

Background

III-Nitrides, with excellent optic and electronic properties, are widely used for solar cells, optical waveguides, high-speed electronics, and terahertz emitters [1]. Among them, InN has the narrowest bandgap, lowest effective mass of electrons, and highest electron mobility and thus can be applied in high-speed electronics [2–4]. However, its low decomposition temperature, impurity-prone surface, and large lattice mismatch with common substrates hinder the further development of InN-based devices [1]. In recent years, many studies focused on the growth of InN nanorods and nanocolumns on c-Al_2O_3, glass, Si (100), and Si (111) with or without buffer layers such as GaN, AlN, InGaN, and even low-temperature (LT) InN [5–10]. In general, sapphire is widely used as the substrate for growth of InN because of its availability, large area, high quality, high thermal stability, relatively low cost, and hexagonal symmetry, even though it has a large lattice mismatch with InN [11].

Selective-area growth (SAG) technique has been used to produce waveguides [12], facet lasers [13], and other nanostructures such as nanowires and nanocolumns [14–16]. It has been applied to achieve the epitaxial lateral overgrowth (ELOG) of GaN-based laser diodes for reducing the threading dislocation density. Until now, there are only a few reports on the SAG of InN, in which Mo-mask-patterned (0001) sapphire [11], Mo-mask-patterned (111) Si [17], nanohole-patterned GaN templates [18], and ultra-thin AlN masks were used [19]. However, the AlN masks are not periodical, and the fabrication of the metal masks is relatively expensive and complex. Hence, more periodical and practical nano-sized masks should be developed for the SAG of InN-based devices.

Anodic aluminum oxide (AAO) templates are widely applied in nanostructure fabrication due to their high regularity, self-organized nanostructure, and low cost compared with electron beam lithography (EBL) [20]. Furthermore, AAO is more easily etched compared to Pt, Mo, and AlN. Therefore, AAO templates were used in this study as both the SAG mask and the transfer template.

Methods

Figure 1 shows the schematic diagram of the fabrication process: High-purity (99.999%) aluminum foils were used to fabricate the AAO templates through a typical two-step anodizing procedure. According to the anodization conditions, the pore diameter and interpore edge-to-edge distance were expected to be 30 and 70 nm, which was shown in Fig. 2a. The depth of AAO pores

* Correspondence: xiaowang25@whu.edu.cn
Key Laboratory of Artificial Micro- and Nano-structures of Ministry of Education, School of Physics and Technology, Wuhan University, Wuhan 430072, People's Republic of China

Springer Open

© The Author(s). 2017 **Open Access** This article is distributed under the terms of the Creative Commons Attribution 4.0 International License (http://creativecommons.org/licenses/by/4.0/), which permits unrestricted use, distribution, and reproduction in any medium, provided you give appropriate credit to the original author(s) and the source, provide a link to the Creative Commons license, and indicate if changes were made.

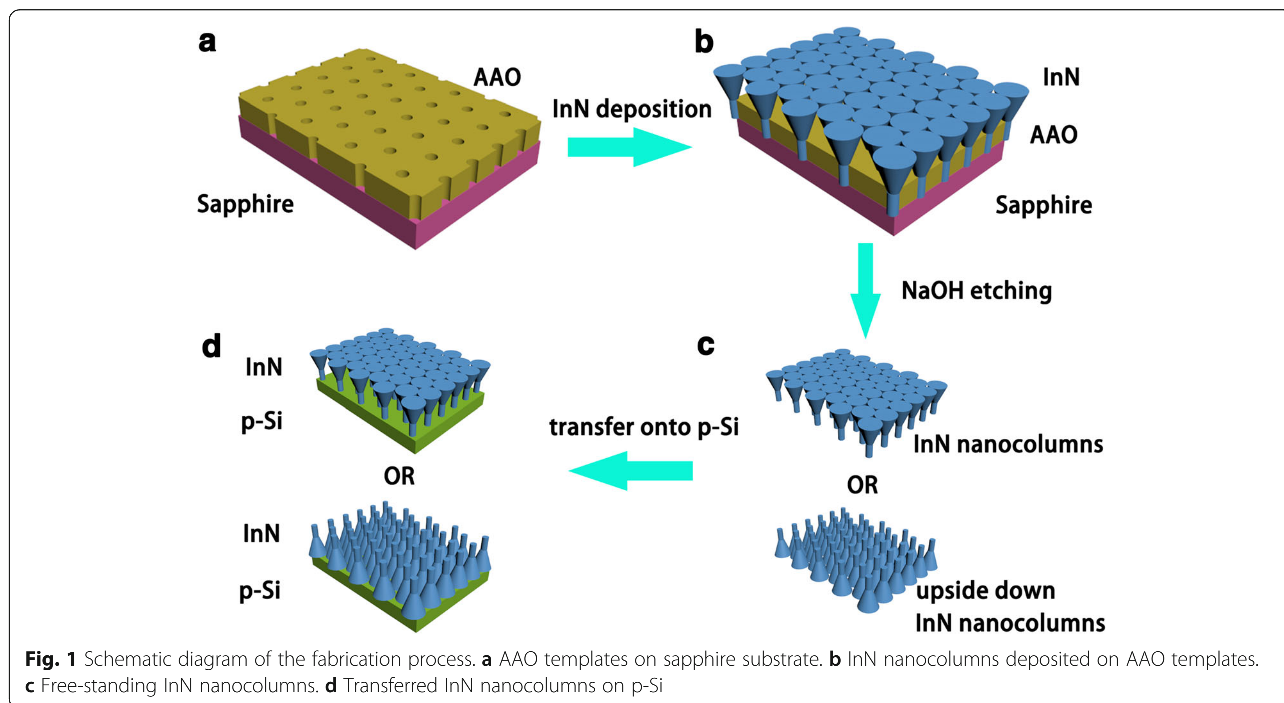

Fig. 1 Schematic diagram of the fabrication process. **a** AAO templates on sapphire substrate. **b** InN nanocolumns deposited on AAO templates. **c** Free-standing InN nanocolumns. **d** Transferred InN nanocolumns on p-Si

was 170 nm. After anodization, the aluminum base and barrier layers were removed completely out and the free-standing AAO templates were transferred onto sapphire substrates. Details of anodization and transferring methods can be found elsewhere [21]. The sapphire wafers used in this work were ultrasonically cleaned in acetone for 10 min and rinsed with ethanol for 10 min to remove organic grease. InN nanocolumns were then grown on sapphire substrates with and without AAO templates for 2 h by radio-frequency molecular beam epitaxy (RF-MBE, SVTA 35-V-2). The temperatures of In source and the substrate were set at the optima 770 and 400 °C, respectively [10]. Prior to the growth, nitridation was performed under 500 W RF-plasma power at 500 °C for 10 min in a nitrogen atmosphere with a flow rate of 2.65 sccm. The InN nanocolumns were characterized by high-resolution X-ray diffraction (HRXRD, Bede D1) and scanning electron microscopy (SEM, FEI, Versa 3D). The as-grown samples were then immerged into NaOH solution with a concentration of 10% at 50 °C for 10 min to remove the AAO templates and then rinsed with deionized water to remove the NaOH solution and reaction products. After NaOH solution etching, the detached InN nanocolumns randomly floated in

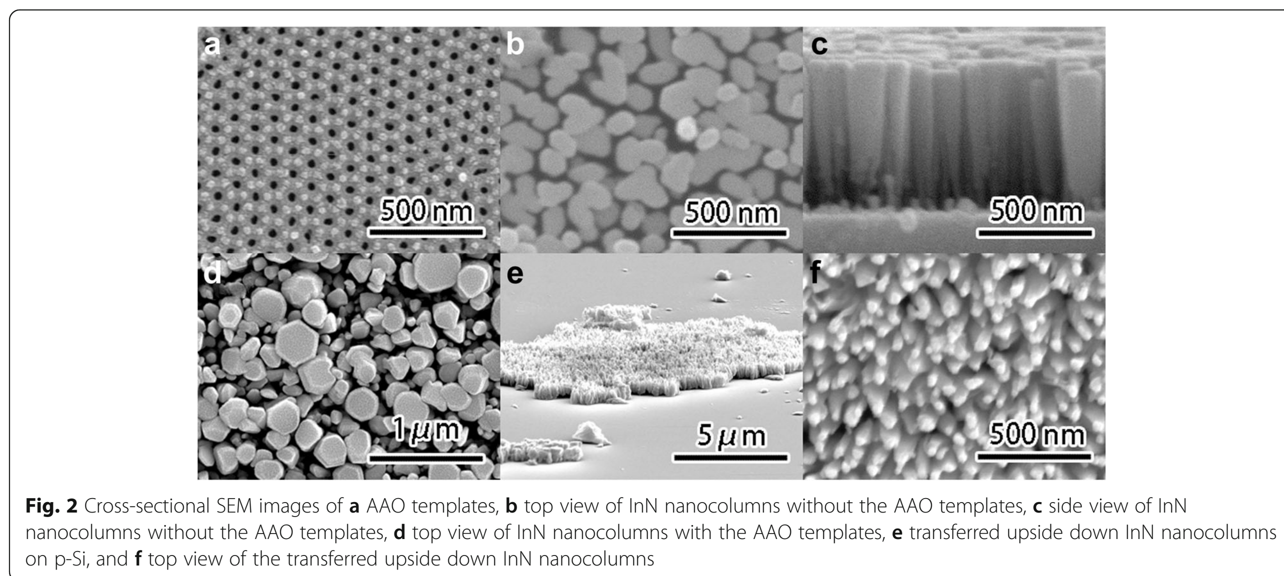

Fig. 2 Cross-sectional SEM images of **a** AAO templates, **b** top view of InN nanocolumns without the AAO templates, **c** side view of InN nanocolumns without the AAO templates, **d** top view of InN nanocolumns with the AAO templates, **e** transferred upside down InN nanocolumns on p-Si, and **f** top view of the transferred upside down InN nanocolumns

the deionized water. The InN nanocolumns were subsequently transferred onto p-Si substrates either in growth direction or upside down. Current versus voltage (I–V) characteristics of the transferred n-InN/p-Si heterojunctions were measured by using a semiconductor device analyzer (Keithley 4200, Keithley Instruments).

Results and Discussion

Figure 2 shows the cross-sectional SEM images. The AAO templates were found with an average pore diameter of 30 nm and interpore edge-to-edge distance of 70 nm as well as pore depth of 170 nm, as shown in Fig. 2a. The density of the pores was estimated to be 1.2×10^{10} cm^{-2}. As shown in Fig. 2b, the diameters of the InN nanocolumns without AAO templates varied from 50 to 150 nm in top view. The density of the InN nanocolumns without the AAO templates was estimated to be 8×10^{9} cm^{-2}. As shown in Fig. 2c, the depth of the nanocolumns was 625 nm. As shown in Fig. 2d, the diameters of the InN nanocolumns with the AAO templates varied from 50 to 500 nm. The density of the InN nanocolumns with the AAO templates was estimated to be 1×10^{9} cm^{-2}. The decrease of the InN nanocolumns densities was mainly attributed to the selective lateral growth by adding the AAO templates. As shown in Fig. 2e, the InN nanocolumns can be either in growth direction or upside down after being transferred onto p-Si by etching AAO templates off using NaOH solution. The sizes of the transferred InN nanocolumns were in micrometer scales from 2×2 to 20×20 μm^2. Fig. 2f shows the top view of the transferred upside down InN nanocolumns. The density of the transferred upside down InN nanocolumns with the AAO templates was estimated to be 1.1×10^{10} cm^{-2}, which was in agreement with the density of the AAO template pores as shown in Fig. 2a. This indicates that the InN nanocolumns were selective-area grown from the pores of the AAO templates.

Figure 3 shows X-ray diffraction (XRD) patterns of the InN nanocolumns with and without the AAO templates. Two peaks were detected in 2θ-ω scan. The peaks around 31.4° and 41.9° were attributed to InN (0002) and sapphire (0006), respectively. It can be clearly seen that the InN (0002) peak with the AAO templates is much sharper compared to that without the AAO templates. This indicates that the crystalline quality of the InN nanocolumns is improved by using the SAG with the AAO templates. Furthermore, the InN (0002) peak with AAO templates shifts to smaller 2 θ region, approaching the native value of the free-standing InN films at 31.3°. The inset shows the rocking curves of InN (0002) with and without AAO templates after normalization. The full widths at half maximum (FWHM) of InN (0002) with and without the AAO templates are 1260″ and 2988″ after fitting with Gaussian curve, respectively,

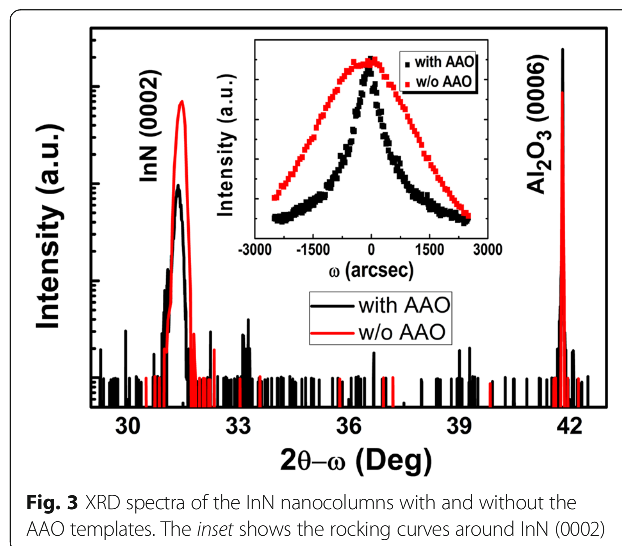

Fig. 3 XRD spectra of the InN nanocolumns with and without the AAO templates. The *inset* shows the rocking curves around InN (0002)

indicating a significantly improved crystalline quality of InN nanocolumns by the SAG using AAO templates.

Figure 4 shows the current–voltage (I–V) characteristic of the transferred n-InN/p-Si heterojunctions. The indium electrodes were welded on the surfaces of the transferred InN and Si layers to achieve ohmic contacts. The inset shows the ohmic contact between the indium electrodes and p-Si. I–V curves were measured by changing the bias from +2 to −2 V. The currents were restricted between 30 and −30 mA to protect the devices. Diode-like behaviors were obtained. Under reverse bias of −2 V, the leakage current of the transferred n-InN/p-Si heterojunctions was about 26 nA, while the current under forward bias of 2 V was about 121 mA. On/off ratio (current ratio I_{pos}/I_{neg} under the positive voltage (+2 V) and negative voltage (−2 V)) was as high as 4.65×10^3, which was much higher than the value reported

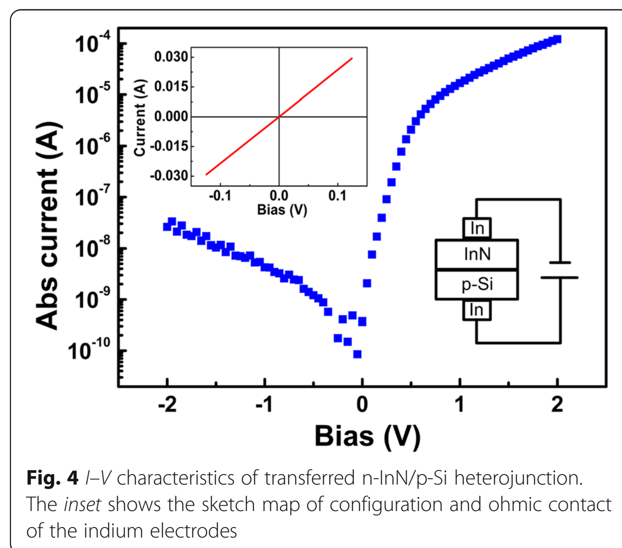

Fig. 4 I–V characteristics of transferred n-InN/p-Si heterojunction. The *inset* shows the sketch map of configuration and ohmic contact of the indium electrodes

previously [22]. This high on/off ratio provides more potential for the application of n-InN/p-Si diodes. Under the forward biases, the turn-on voltage of the transferred n-InN/p-Si heterojunctions was fitted to be 0.67 V, which was comparable to the average barrier height of 0.7 V in Bhat's work [22]. Thus, the excellence of the transferred InN nanocolumns and the n-InN/p-Si heterojunctions can be deduced.

Conclusions

In this study, InN nanocolumn arrays were grown on c-plane sapphire with and without the AAO nanotemplates. The crystalline quality of the InN nanocolumns is significantly improved by the SAG using the AAO nanotemplates, as verified by XRD measurements. *I*–*V* characteristic of the transferred n-InN/p-Si heterojunctions shows on/off ratio as high as 4.65×10^3 at 2 V. This work offers a potential way to grow high-quality transferable devices with improving performances.

Acknowledgements
This work is supported by the NSFC under Grant No. 11574235 and the MOST China under Grant No. 2014GB109004. The authors would like to thank Dr. C. Chen for the technical support.

Authors' Contributions
XW carried out the experiments and drafted the manuscript. GZZ and YX participated in the measurements. HW conceived the study and participated in its design. CL supervised the overall study and polished the manuscript. All authors read and approved the final manuscript.

Competing Interests
The authors declare that they have no competing interests.

Received: 29 December 2016 Accepted: 14 February 2017
Published online: 23 February 2017

References

1. Bhuiyan AG, Hashimoto A, Yamamoto A (2003) Indium nitride (InN): a review on growth, characterization, and properties. J Appl Phys 94:2779–2808
2. Matsuoka T, Okamoto H, Nakao M, Harima H, Kurimoto E (2002) Optical bandgap energy of wurtzite InN. Appl Phys Lett 81:1246–1248
3. Klochikhin AA, Davydov VY, Emtsev VV, Sakharov AV, Kapitonov VA, Andreev BA, Lu H, Schaff WJ (2005) Acceptor states in the photoluminescence spectra of n-InN. Phys Rev B 71:195207
4. Wang X, Zhang GZ, Xu Y, Gan XW, Chen C, Wang Z, Wang Y, Wang JL, Wang T, Wu H, Liu C (2016) Leakage current mechanism of InN-based metal-insulator-semiconductor structures with Al_2O_3 as dielectric layers. Nanoscale Res Lett 11:21
5. Li H, Zhao G, Wei H, Wang L, Chen Z, Yang S (2016) Growth of well-aligned InN nanorods on amorphous glass substrates. Nanoscale Res Lett 11:270
6. Grandal J, Sánchez-García MA, Calleja E, Luna E, Trampert A (2007) Accommodation mechanism of InN nanocolumns grown on Si(111) substrates by molecular beam epitaxy. Appl Phys Lett 91:021902
7. Calleja E, Grandal J, Sánchez-García MA, Niebelschütz M, Cimalla V, Ambacher O (2007) Evidence of electron accumulation at nonpolar surfaces of InN nanocolumns. Appl Phys Lett 90:262110
8. Wang KR, Lin SJ, Tu LW, Chen M, Chen QY, Chen TH, Chen ML, Seo HW, Tai NH, Chang SC, Lo I, Wang DP, Chu WK (2008) InN nanotips as excellent field emitters. Appl Phys Lett 92:123105
9. Xu HY, Liu Z, Zhang XT, Hark SK (2007) Synthesis and optical properties of InN nanowires and nanotubes. Appl Phys Lett 90:113105
10. Pan Y, Wang T, Shen K, Peng T, Wu K, Zhang W, Liu C (2010) Rapid growth and characterization of InN nanocolumns on InGaN buffer layers at a low ratio of N/In. J Cryst Growth 313:16–19
11. Kamimura J, Kishino K, Kikuchi A (2010) Dislocation reduction via selective-area growth of InN accompanied by lateral growth by rf-plasma-assisted molecular-beam epitaxy. Appl Phys Lett 97:141913
12. Tanaka T, Uchida K, Watanabe A, Minagawa S (1996) Selective growth of gallium nitride layers with a rectangular cross-sectional shape and stimulated emission from the optical waveguides observed by photopumping. Appl Phys Lett 68:976–978
13. Akasaka T, Ando S, Nishida T, Saito H, Kobayashi N (2001) Room-temperature lasing of InGaN multiquantum-well hexagonal microfacet lasers by current injection. Appl Phys Lett 79:1414–1416
14. Hersee SD, Sun X, Wang X (2006) The controlled growth of GaN nanowires. Nano Lett 6:1808–1811
15. Ishizawa S, Kishino K, Kikuchi A (2008) Selective-area growth of GaN nanocolumns on Si(111) substrates using nitrided Al nanopatterns by RF-plasma-assisted molecular-beam epitaxy. Appl Phys Express 1:015006
16. Kishino K, Sekiguchi H, Kikuchi A (2009) Improved Ti-mask selective-area growth (SAG) by rf-plasma-assisted molecular beam epitaxy demonstrating extremely uniform GaN nanocolumn arrays. J Cryst Growth 311:2063–2068
17. Denker C, Malindretos J, Landgraf B, Rizzi A (2009) Catalyst-free selective area growth of InN nanocolumns by MBE. Cond-Mat Mtrl-Sci arXiv:0905.3133v1
18. Harui S, Tamiya H, Akagi T, Miyake H, Hiramatsu K, Araki T, Nanishi Y (2008) Transmission electron microscopy characterization of position-controlled InN nanocolumns. Jpn J Appl Phys 47:5330–5332
19. Wang K, Araki T, Takeuchi M, Yoon E, Nanishi Y (2014) Selective growth of N-polar InN through an in situ AlN mask on a sapphire substrate. Appl Phys Lett 104:32108
20. Masuda M, Fukuda K (1995) Ordered metal nanohole arrays made by a two-step replication of honeycomb structures of anodic alumina. Science 268:1466–1468
21. Ding GQ, Zheng MJ, Xu WL, Shen WZ (2005) Fabrication of controllable free-standing ultrathin porous alumina membranes. Nanotechnology 16:1285–1289
22. Bhat TN, Roul B, Rajpalke MK, Kumar M, Krupanidhi SB, Sinha N (2010) Temperature dependent transport behavior of n-InN nanodot/p-Si heterojunction structures. Appl Phys Lett 97:202107

Submit your manuscript to a SpringerOpen journal and benefit from:

- ► Convenient online submission
- ► Rigorous peer review
- ► Immediate publication on acceptance
- ► Open access: articles freely available online
- ► High visibility within the field
- ► Retaining the copyright to your article

Submit your next manuscript at ► springeropen.com